The Astrophysical Journal, 849:79 (7pp), 2017 November 10 https://doi.org/10.3847/1538-4357/aa8e49

Correlation between Angular Widths of CMEs and Characteristics of Their Source Regions

X. H. Zhao[1,2], X. S. Feng[1,2], H. Q. Feng[3], and Z. Li[4]
[1] State Key Laboratory of Space Weather, National Space Science Center, Chinese Academy of Sciences, Beijing 100190, China
[2] HIT Institute of Space Science and Applied Technology, Shenzhen 518055, China
[3] Institute of Space Physics, Luoyang Normal University, Luoyang, Henan 471934, China
[4] Institute of Space Weather, Nanjing University of Information Science & Technology, Nanjing, Jiangsu 210044, China
Received 2016 October 31; revised 2017 September 19; accepted 2017 September 19; published 2017 November 3

Abstract

The angular width of a coronal mass ejection (CME) is an important factor in determining whether the corresponding interplanetary CME (ICME) and its preceding shock will reach Earth. However, there have been very few studies of the decisive factors of the CME's angular width. In this study, we use the three-dimensional (3D) angular width of CMEs obtained from the Graduated Cylindrical Shell model based on observations of *Solar Terrestrial Relations Observatory* (*STEREO*) to study the relations between the CME's 3D width and characteristics of the CME's source region. We find that for the CMEs produced by active regions (ARs), the CME width has some correlations with the AR's area and flux, but these correlations are not strong. The magnetic flux contained in the CME seems to come from only part of the AR's total flux. For the CMEs produced by flare regions, the correlations between the CME angular width and the flare region's area and flux are strong. The magnetic flux within those CMEs seems to come from the whole flare region or even from a larger region than the flare. Our findings show that the CME's 3D angular width can be generally estimated based on observations of *Solar Dynamics Observatory* for the CME's source region instead of the observations from coronagraphs on board the *Solar and Heliospheric Observatory* and*STEREO* if the two foot points of the CME stay in the same places with no expansion of the CME in the transverse direction until reaching Earth.

Key words: solar–terrestrial relations – Sun: coronal mass ejections (CMEs) – Sun: flares – sunspots

1. Introduction

Coronal mass ejections (CMEs) refer to the large-scale release of plasma and the magnetic field from the Sun and their propagation in interplanetary space. If the corresponding interplanetary CMEs (ICMEs) contain a strong and long duration southward magnetic field component within their internal structures, they will lead to non-recurrent geomagnetic storms when colliding with Earth's magnetosphere (Gosling 1993; Dryer 1994; Green & Baker 2015). CMEs are believed to be major sources of extreme space weather events, and become one of the objectives most concerned in the space weather study. Generally speaking, the geoeffects of CMEs can be divided into three aspects, i.e., whether they will encounter Earth, when they will arrive if they could, and how strong the geomagnetic disturbances that they introduce will be. As far as the first issue is concerned, many statistical studies have demonstrated that not all CMEs coming from the front side of the Sun (the side facing Earth) will reach Earth (Cane et al. 2000; St. Cyr et al. 2000; Webb et al. 2000; Wang et al. 2004; Zhao et al. 2006). The angular width of the CME, i.e., its spatial span relative to the Sun center, is one of the most important factors contributing to whether the ICME would be able to encounter Earth. The 2010 January 2 CME event is an example. The half angular width of this CME was 35°, and its main propagation direction was more than 50° away from the *Solar Terrestrial Relations Observatory* (*STEREO*) and L1 spacecraft. Therefore, Zhao et al. (2010) predicted that this CME could reach neither the *STEREO-A/B*nor the L1 spacecraft, which was witnessed by in situ measurements of spacecraft.

Previous studies demonstrated that the CME plasmoid keeps in lateral pressure balance with the surrounding magnetic field beyond some height in or below the outer corona, and that the CME's angular width remains constant after the critical height (Moore et al. 2007; Zhao et al. 2010). This critical height is usually several solar radii. The CME width is usually estimated from the projected angular width, i.e., the span angle between the two position angles of the CME's outer edges relative to the Sun center in the coronagraph's plane of sky (POS). Besides the contribution to whether the CME could reach Earth, the angular width also determines the spatial extent of the CME's preceding shock. The shock's spatial extent, on the other hand, determines the spatial extent where the solar energetic particles (SEPs) are accelerated and the SEP's duration time (Kahler 2004, 2005; Pan et al. 2011). Wider CMEs have a higher probability to disturb magnetic fields in the solar corona, and therefore have a higher probability to be associated with type II bursts (Raymond et al. 2000; Gopalswamy et al. 2001; Pick et al. 2006). Kahler & Gopalswamy (2009) found that only CMEs with projected angular width greater than 60° are associated with type II events or gradual SEP events at 1 au.

We can see that angular width is an important parameter as far as the CME's space weather effect is concerned. Therefore, it is necessary to investigate how angular width correlates with other parameters of the CME and how to predict it based on observations of the relevant observables. Burlaga et al. (1981) found that the legs of CMEs are still connected to the Sun and that they lie on both sides of the neutral line in their source regions when CMEs propagate into interplanetary space. Therefore, the angular width of a CME should be controlled by some characteristics of its source region. Moore et al. (2007)

used the theoretical model to study relations between the final angular width of the CME after its lateral expansion phase and the magnetic flux of its producing source region. They found that a CME's final angular width could be estimated from the magnetic flux covered by its source region flare arcade. They applied this relation to three well-observed CMEs erupting from flare regions, and found good agreements. Kim et al. (2008) examined 105 front-side halo CMEs during 1996–2001 with source regions located near the disk center, and found that 74% (78/105) of the sample events show multiple-flux system features. This demonstrates that multiple-flux systems are far more heavily involved in wider CMEs than single-flux systems. Chen et al. (2011a) investigated 71 limb CMEs produced by active regions (ARs) and found that the area and total magnetic flux of the AR have strong correlations with the angular width of CMEs; The correlation coefficient (C.C.) between the linear combination of the AR's area and flux and the corresponding CME's angular width is 0.45. Kwon et al. (2015) studied 62 halo CMEs during 2010–2012 based on the stereoscopic observations from the *STEREO* and *Solar and Heliospheric Observatory* (*SOHO*) spacecraft. They concluded that the apparent width of halo or partial halo CMEs is determined by the existence and extent of the associated waves or shocks and does not represent an accurate measure of the ejecta size. Correlations between the CME angular width and other structures and/or activities, such as the scale of magnetic loop (Klimchuk et al. 1994; Chen et al. 2006, 2011b), the X-ray flux of the associated flare (Kahler et al. 1989; Vršnak et al. 2005), and the width of the closed field line regions have also been reported.

In previous studies, the CME angular width was obtained from the POS of *SOHO*/LASCO. The width obtained in this way is the projected angular width of CMEs on the two-dimensional (2D) plane (i.e., POS) and does not represent the real width of CMEs in 3D space. Now, some 3D reconstruction methods have been developed to get the real 3D morphologies of CMEs based on multi-spacecraft observations including *STEREO* and *SOHO*, such as the Graduated Cylindrical Shell (GCS) modeling technique developed by Thernisien et al. (2006). From these methods, we can obtain a CME's width in 3D space rather than the projected ones in past studies. We use the 3D angular-width values of CMEs in this study because they deal with the CME's intrinsic properties. On the other hand, the *Solar Dynamics Observatory* (*SDO*) can provide accurate magnetic data for the CME's source region, which enables us to get the source region's characteristics of CMEs. Then potential relations between them will be investigated in this study.

2. Data

2.1. The 3D Angular Width OF CMES

The *STEREO*/SECCHI/COR2 CME Database developed by the Institute for Astrophysics, University of Goettingen, Germany, currently provides information on 1060 bright CMEs from 2007 January until the end of 2011 December. Out of a selected set of 264 CMEs, which appeared very clear in brightness and structure, 241 were analyzed with the GCS model. Bosman et al. (2012) first reported the 3D properties of these CMEs based on the 3D modeling technique. A full list of these CMEs is available at http://www.affects-fp7.eu/cme-database/database.php. For each of the 241 events, the GCS model was applied to reconstruct the 3D shape of the CME and obtain the half-angle alpha of GCS flux rope, which is the half angular width of the CME in 3D space. These angular widths were obtained when the CME front had reached 10–20 solar radii. Therefore, they usually denote the final widths of CMEs as the CME's lateral expansion becomes smaller after these distances (Moore et al. 2007; Zhao et al. 2010). Among these 241 events, there are 165 with clearly identified source regions of the associated CMEs. *SDO* started to provide magnetic data from 2011 May, so we selected the events after 2011 May from these 165 events with source regions. The source regions can be divided into four types: active regions (ARs), prominence (P), flare (F), and post eruptive arch (PEA). For some events, the source region type is not so clear (these are denoted with "?" in the web). Some events have mixed source region types, such as AR and PEA, and P and AR. In this way, we get 23 CME events produced by ARs during 2010.05–2011.12 (Table 1), and 10 CME events produced by flare regions during 2011.05–2011.09 (Table 2). Column 4 in Tables 1 and 2 gives the half angular width of the CME reconstructed from the GCS model based on observations of the twin *STEREO* spacecraft. This parameter is better than the projected angular width in the POS of *SOHO*/LASCO. Column 9 in Table 1 gives the AR's area (in micro-hemisphere, i.e., millionths) and column 10 gives the AR's magnetic flux (in weber). How to compute these two parameters will be shown in the next section. B_R(1 au) is the strength of the radial component of the interplanetary magnetic field at 1 au detected by *Wind* spacecraft at the GCS modeling time. This parameter will be used to validate the relation between the CME's angular width and characteristics of its source region.

2.2. Source Region's Area and Magnetic Flux

For each event in Table 1, we downloaded the so called Space-weather Helioseismic and Magnetic Imager (HMI) Active Region Patches (SHARPs) data product by the *SDO*'s HMI from the Joint Science Operations Center (JSOC) web (http://jsoc.stanford.edu/ajax/lookdata.html?ds=hmi.sharp_cea_720s). The SHARP data series, which automatically calculate indices to characterize ARs with a 12-minute cadence, provide a systematic AR database of patches of photospheric vector magnetic field, Doppler velocity, continuum intensity, and line-of-sight magnetic field from full-disk data (Bobra et al. 2014). The AR parameters are stored as keywords in the SHARP data. We use the "hmi.sharp_cea_720s series" of the SHARP data in this study, which is definitive data with 11 segments wherein all quantities have been remapped from CCD coordinates to a heliographic Cylindrical Equal-area (CEA) coordinate system centered on the patch (Bobra et al. 2014). Therefore, the area parameter in this data series needs no more corrections. READ_SDO.PRO in the solar software (SSW) is adopted to read these SHARP data. Then, the returned header structure "header.AREA_ACR" provides the de-projected area of the AR (in micro-hemisphere), and "header.USFLU" provides the total unsigned flux of the AR (in weber). The AR's area and magnetic flux obtained in this way are shown in columns 9 and 10 of Table 1, respectively.

The HMI magnetic data for the whole Sun was downloaded from http://jsoc.stanford.edu/ajax/exportdata.html. The AIA 304 Å data was also obtained from this web. We need to specify the location and area of the flare region from AIA observations, and compute the magnetic flux in the corresponding

Table 1
Twenty-three CMEs Produced by Active Regions (ARs)

Event No.*	Date of GCS Modeling	Time of GCS Modeling	Half Angular Width	NOAA No.	Active Region No.	Sunspot Location	Source Region Kind	Active Region Area (millionths)	Active region Total Flux (weber)	B_R(1 au) (nT)
1	2010 May 23	22:08:15	13.98	11072	26	S16W06	AR	361.7	5.47×10^{13}	2.0
2	2010 May 24	17:08:15	20.12	11072	26	S15W23	AR	337.4	4.8×10^{13}	1.0
3	2010 Jun 21	03:08:15	15.65	11082	57	N27W19	AR	279.2	3.45×10^{13}	1.5
4	2010 Aug 01	10:08:15	23.20	11092	104	N13E21	AR	597.0	1.29×10^{14}	3.0
5	2011 Jan 30	20:08:15	11.74	11150	355	S22E36	AR	388.1	9.3×10^{13}	2.5
6	2011 Feb 02	02:08:15	33.54	11150	355	S22W03	AR	449.0	6.21×10^{13}	2.0
7	2011 May 16	23:08:15	14.81	11172	421	N10E03	AR	443.4	5.23×10^{13}	1.5
8	2011 Apr 07	14:08:15	15.37	11186	480	N22E44	AR	755.0	2.65×10^{14}	1.0
9	2011 Apr 08	03:08:15	22.92	11184	466	N16W55	AR	624.4	2.46×10^{14}	2.0
10	2011 Apr 12	06:08:15	38.57	11186	480	N23W08	AR	1250.3	2.67×10^{14}	4.0
11	2011 Apr 17	10:08:15	10.90	11191	504	N08E17	AR	1328.0	3.02×10^{14}	2.0
12	2011 Apr 25	02:08:15	17.89	11196	533	S26E26	AR	25.9	2.97×10^{12}	2.0
13	2011 May 06	12:08:15	50.87	11204	556	N17W14	AR	1127.9	1.99×10^{14}	1.0
14	2011 Jun 01	22:08:15	23.76	11226	637	S22E15	AR	1353.6	2.94×10^{14}	2.0
15	2011 Jun 13	06:08:15	21.80	11234	661	S15E04	AR	264.9	2.94×10^{13}	3.0
16	2011 Aug 13	15:08:15	10.62	11266	759	N20W88	AR	40.0	4.05×10^{13}	1.0
17	2011 Sep 15	03:08:15	12.58	11294	854	S17W16	AR	303.9	5.14×10^{13}	3.0
18	2011 Sep 22	00:08:15	18.73	11296	856	N26W29	AR	2034.9	5.55×10^{14}	4.0
19	2011 Sep 25	12:08:15	6.43	11303	899	S28W80	AR	606.6	2.44×10^{14}	4.0
20	2011 Sep 29	23:08:15	9.78	11304	900	N13W47	AR	79.5	2.37×10^{13}	3.0
21	2011 Nov 12	23:08:15	22.64	11343	1046	N26W02	AR	532.2	1.01×10^{14}	1.5
22	2011 Nov 26	09:08:15	44.16	11353	1093	N08W49	AR	2511.0	4.07×10^{14}	2.0
23	2011 Dec 23	09:08:15	15.65	11381	1210	S18W42	AR	835.9	1.78×10^{14}	2.0

Note. Columns 1–4 and Column 8 are taken from http://www.affects-fp7.eu/cme-database/database.php (the *STEREO*/SECCHI/COR2 CME database developed by the Institute for Astrophysics, University of Goettingen, German). Column 5 is the NOAA number for the active region, taken from https://solarmonitor.org/; Column 6 is the active region number for download *SDO* data (http://jsoc.stanford.edu/data/hmi/HARPs_movies/definitive.) AR in column 8 stands for active region. Column 9 and column 10 denote the active region area and total magnetic flux, respectively; they are obtained from the header structure after we apply the READ_SDO.PRO subroutine to read the active region data. Column 11 is the strength of the radial component of the interplanetary magnetic field at 1 au detected by the *Wind* spacecraft at the GCS modeling time.

Table 2
Ten CMEs Produced by Flare Regions during 2011.05–2011.09

Event No.*	Date of GCS Modeling	Time of GCS Modeling	Half Angular Width	NOAA No.	Active Region No.	Sunspot Location	Source Region Kind	Active Region Area (millionths)	Active Region total flux (weber)	B_R(1 au) (nT)
24	2011 May 29	15:08:15	53.11	11226	637	S19E53	F/AR	1056.3	1.34×10^{13}	2.0
25	2011 Jun 08	14:08:15	12.58	11226	637	S21W78	F(AR)	791.0	4.11×10^{12}	3.0
26	2011 Aug 04	05:08:15	62.89	11261	750	N16W51	P/F	900.0	1.91×10^{13}	2.0
27	2011 Sep 07	01:08:15	35.50	11283	833	N14W18	F/P	625.0	1.03×10^{13}	2.5
28	2011 Sep 08	02:08:15	15.93	11283	833	N14W32	F/P	625.0	4.69×10^{12}	2.0
29	2011 Sep 09	00:08:15	44.44	11283	833	N14W46	AR/F	791.0	1.51×10^{13}	4.0
30	2011 Sep 09	13:08:15	19.29	11283	833	N16W56	AR/F	564.1	8.48×10^{12}	4.0
31	2011 Sep 10	13:08:15	34.94	11283	833	N17W69	F/AR	625.0	1.25×10^{13}	4.0
32	2011 Sep 22	12:08:15	18.73	11302	892	N11E60	AR/F	534.8	2.72×10^{12}	3.0
33	2011 Sep 24	14:08:15	26.83	11302	892	N13E45	AR/F	791.0	1.83×10^{13}	3.5

Note. Columns 1–8, and column 11 are the same as those in Table 1. In column 8, F stands for Flare, AR stands for active region, and P stand for prominence. Columns 9 and 10 denote the area and total magnetic flux of the flare region that we compute; how to get them is given in Section 2.

locations on HMI magnetogram. Figure 1 shows an example. The left panel displays the observation of AIA 304 Å for the 2011.09.07 CME event. The source location of this CME is N14W18 (see Table 2). We can find a bright patch around the source location in the AIA picture. Then, we draw by hand a minimum circle to encircle this bright patch to specify the location and scope of the flare region. For each pixel within the circle, we compute its de-projected area (in micro-hemisphere):

$$A_i = \frac{A_p 10^6}{2\pi R_s^2 \cos(d_i)} = \frac{A_p 10^6}{2\pi R_s^2 \cos(\theta_i)\cos(\varphi_i)}, \quad (1)$$

where A_p is the pixel's area on the surface of the Sun located in the disk center; R_s is the solar radius; d_i is the angular distance

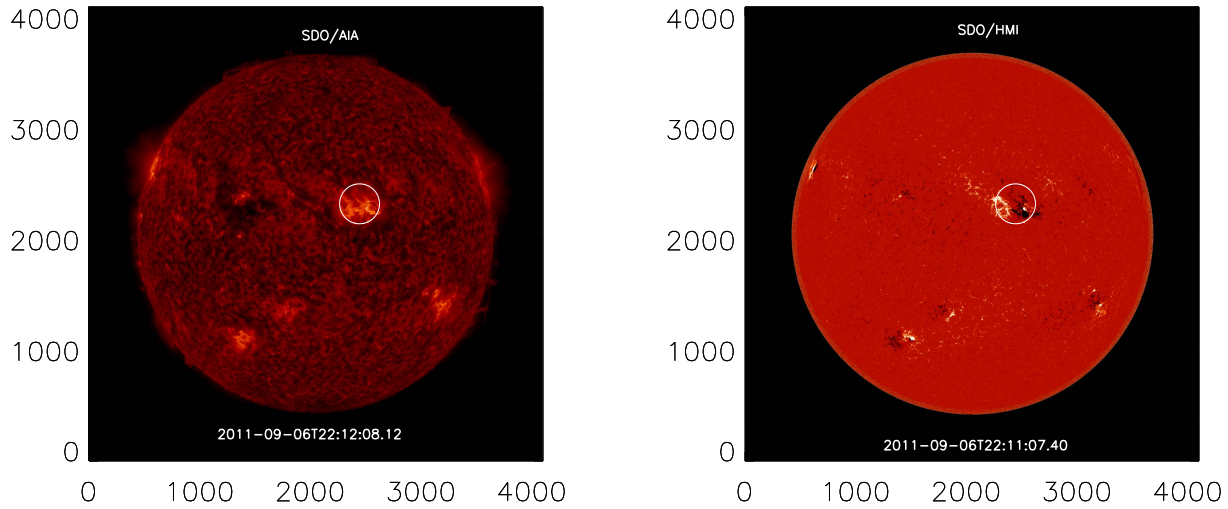

Figure 1. *SDO* AIA 304 Å imaging observation (left panel) and HMI magnetogram (right panel) for the 2011.09.07 CME event. The white circle includes the flare region in AIA imaging, and the reproductive circle in HMI magnetogram shows us the specified region with which to compute the magnetic flux of the flare region.

from the pixel to the disk center; θ_i and φ_i denote its heliographic latitude and longitude, respectively. Then, the area of the flare region ($A_{\rm Flare}$) is computed as the sum of each pixel:

$$A_{\rm Flare} = \sum_{i=1}^{n} A_i, \tag{2}$$

where n is the total number of the pixels. A reproductive circle is drawn on the HMI magnetogram (right panel of Figure 1). The total unsigned magnetic flux within this circle is computed as the total flux of the flare region:

$$\phi_{\rm Flare} = \sum_{i=1}^{n} A_i |B_{{\rm r},i}|, \tag{3}$$

where $B_{{\rm r},i}$ is the radial magnetic field at each pixel within the circle. The flare region's area (in millionths) and magnetic flux (in weber) obtained in this way are given in columns 9 and 10 of Table 2.

3. Results

3.1. CME Angular Width and AR's Characteristics

According to the model proposed by Moore et al. (2007), the CME's final angular width ($\theta_{\rm CME}$) can be determined from its source region flux based on the conservation of the flux (derived from the combination of Equations (16) and (19) in Moore et al. 2007):

$$\theta_{\rm CME} = \frac{1}{1\ {\rm au}} \sqrt{\frac{\phi_{\rm S}}{B_{\rm R}(1\ {\rm au})}}, \tag{4}$$

where $\phi_{\rm S}$ is the magnetic flux of the CME's source region, and $B_{\rm R}(1\ {\rm au})$ is the strength of the radial component of the interplanetary magnetic field at 1 au. We get $B_{\rm R}(1\ {\rm au})$ from the in situ measurements of *Wind* spacecraft at the GCS modeling time. We need to note that this equation applies to the CMEs that are assumed to keep their constant spatial extents after the initial expansion and would not expand any more in the transverse direction in interplanetary space. The predicted angular width by Equation (4) is the CME's real erupting angle instead of a projected one. For the 23 AR-produced CMEs, $\phi_{\rm S}$ should be related to the AR's flux $\phi_{\rm AR}$. As we do not know how to obtain $\phi_{\rm S}$, we use $\phi_{\rm AR}$ instead and check its relation to $\theta_{\rm CME}$. The C.C. between $\theta_{\rm CME}$ and $\sqrt{\frac{\phi_{\rm AR}}{B_{\rm R}(1\ {\rm au})}}$ is 0.40, shown in Figure 2 (top panel). This demonstrates that there does exit some relations between CME width and AR's flux, but the correlations between them are not as strong as we anticipate. The p-value of this correlation is close to 0.05 (the critical value of C.C. is 0.41 on the 0.05 level), demonstrating that the correlation between them is approximately significant. The correlations between $\theta_{\rm CME}$ and $\sqrt{\phi_{\rm AR}}$, $A_{\rm AR}$ (area of AR) are also investigated and shown in the middle and bottom panels of Figure 2. We can see that the correlation between $\theta_{\rm CME}$ and $\sqrt{\phi_{\rm AR}}$ is weak (C.C. = 0.32, p-value close to 0.1), but that the correlation between $\theta_{\rm CME}$ and $A_{\rm AR}$ is strong (C.C. = 0.52, p-value close to 0.01). Therefore, only the AR's area has a strong correlation with the angular width for the CMEs produced by ARs.

To check the model of Moore et al. (2007), we use Equation (4) to predict the CME's angular width based on the AR flux. Figure 3 (top panel) gives the predicted angular width along the 3D reconstructed ones. We can see that the predicted widths are usually wider than the 3D reconstructed ones. Supposing that the model is correct, the wider predicted widths seem to indicate that the flux within the CMEs may come from only part of the ARs. In other words, not all magnetic flux in the ARs will contribute to form the flux within the CMEs. This explains why the C.C. between them is only 0.40 with the p-value of nearly 0.05, not as high as we would expect. Kim et al. (2008) speculated that only part of the magnetic flux in an AR would be ejected during the CME's eruption. Our findings here support their speculations.

3.2. CME Angular Width and Flare Region's Characteristics

For the 10 CMEs produced by flare regions in Table 2, we take the magnetic flux of the flare region as the CME's source region flux ($\phi_{\rm S}$), so we check the C.C. between the CME angular width ($\theta_{\rm CME}$) and the flare region's area ($A_{\rm Flare}$) and flux ($\phi_{\rm Flare}$). It is found that the correlation between $\theta_{\rm CME}$ and $\sqrt{\frac{\phi_{\rm Flare}}{B_{\rm R}(1\ {\rm au})}}$ is the

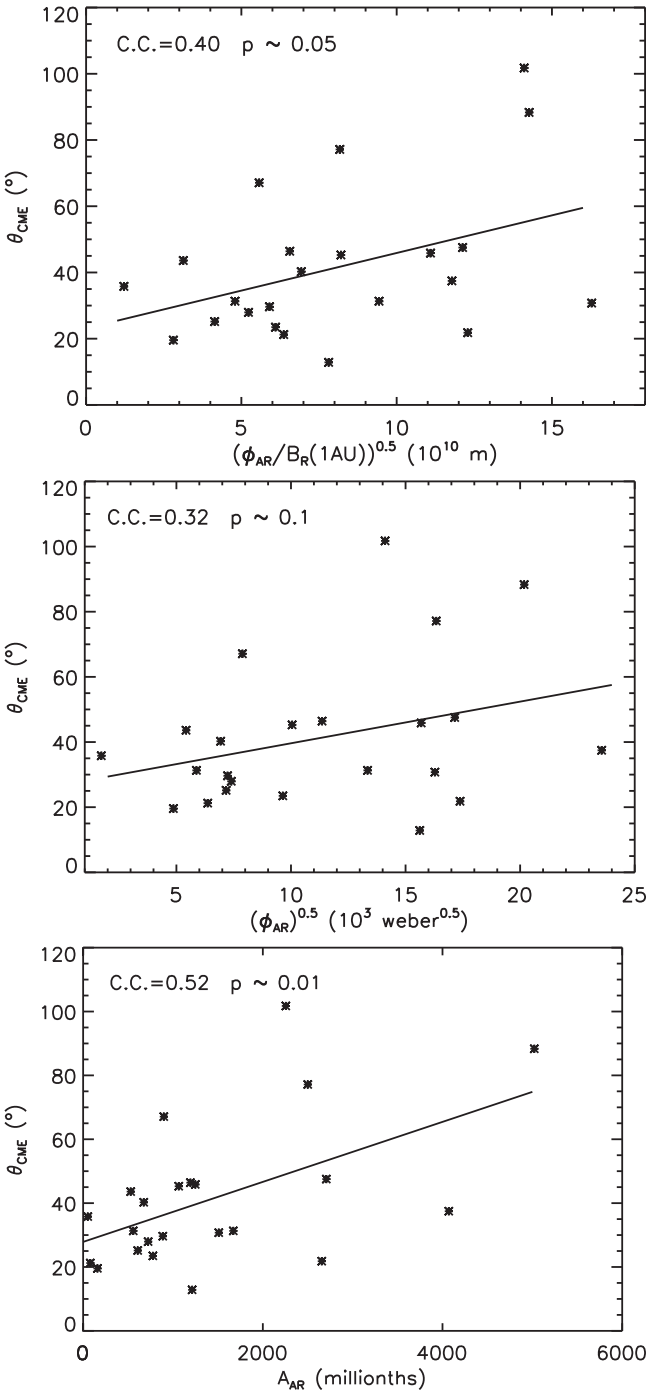

Figure 2. Correlation coefficient (C.C.) between $\theta_{\rm CME}$ and $\sqrt{\frac{\phi_{\rm AR}}{B_R(1\ {\rm au})}}$ (top panel); $\sqrt{\phi_{\rm AR}}$ (middle panel); and $A_{\rm AR}$ (bottom panel) for 23 AR-produced CMEs. Solid lines represent the line fitting.

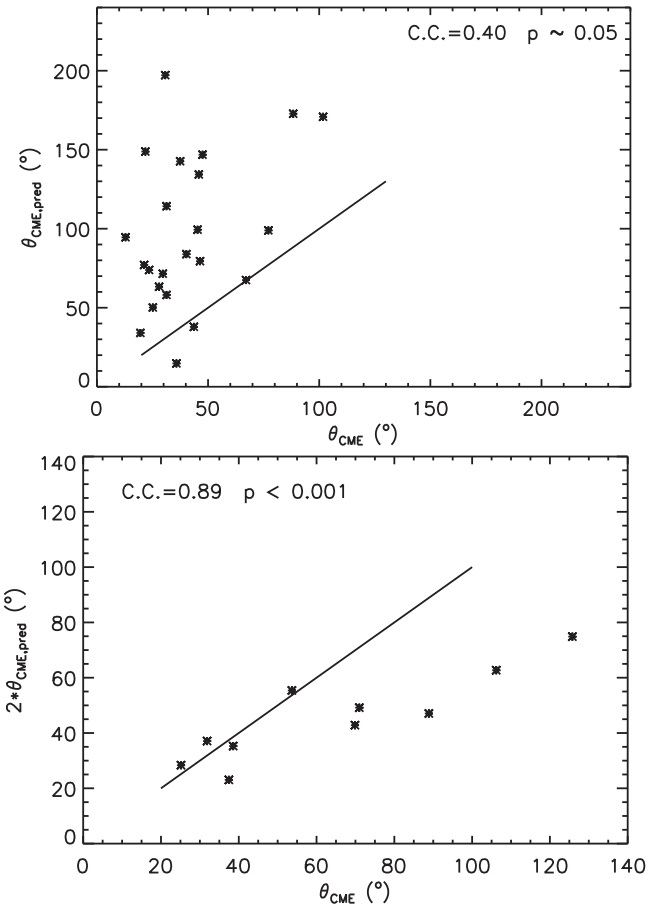

Figure 3. Top panel: the predicted CME angular width ($\theta_{\rm CME,pred}$) based on Equation (4) with ARs as the CME source plotted vs. the reconstructed 3D angular width ($\theta_{\rm CME}$) for 23 AR-produced CMEs; the solid line represents $\theta_{\rm CME,pred} = \theta_{\rm CME}$. Bottom panel: the predicted CME angular width with double ($2\theta_{\rm CME,pred}$) based on Equation (4) with flare regions as the CME source plotted vs. the reconstructed 3D angular width ($\theta_{\rm CME}$) for 10 flare-produced CMEs; the solid line represents $2\theta_{\rm CME,pred} = \theta_{\rm CME}$.

strongest with the C.C. of 0.89 (p-value < 0.001), shown in the top panel of Figure 4. The C.C. between $\theta_{\rm CME}$ and $\sqrt{\phi_{\rm Flare}}$ is 0.78 (p-value < 0.01), shown in the middle panel of Figure 4. The C.C. between $\theta_{\rm CME}$ and $A_{\rm Flare}$ is 0.68 (p-value < 0.05), shown in the bottom panel of Figure 4. We can say that all of these correlations are significant. In contrast with the AR's characteristics, the flare region's characteristics (flux and area) have stronger correlations with the CME's 3D angular width. This means that the CMEs produced by the flare regions have closer relations with the flare regions than that between the AR-produced CMEs and their source ARs.

Similarly, we use Equation (4) to predict the CME angular width based on the flare region flux. It is found that the predicted values are usually only half (even less) of the reconstructed values. Figure 3 (bottom panel) gives the variations of the doubled angular width predicted by Equation (4) along the 3D reconstructed ones. The C.C. between them is 0.89 with the p-value < 0.001. The narrower predicted widths seem to indicate that the flux within the CMEs is larger than the flux within the flare region. In other words, the magnetic flux in the CMEs may come from a larger region than the source flare for these flare-produced CMEs.

4. Conclusion and Discussions

The importance of CMEs in space weather context is widely accepted. As far as the related space weather prediction is concerned, previous studies mainly emphasize CME's propagation speed and its internal magnetic field. Speed contributes to its arrival time, and magnetic field determines largely the corresponding geomagnetic disturbances produced by the CME when colliding with our Earth's magnetosphere. However, little attention is paid to another important parameter of CMEs, i.e., angular width. The real angular width of CMEs in 3D space

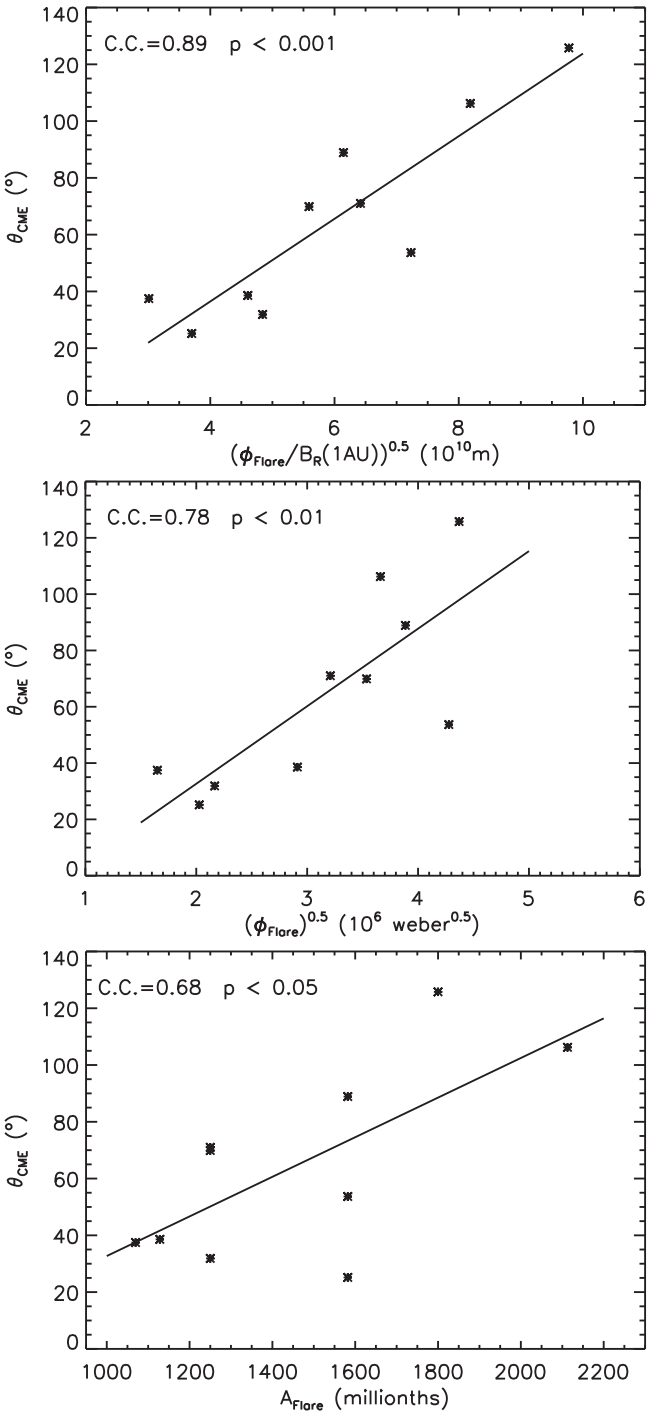

Figure 4. The C.C. between θ_{CME} and $\sqrt{\frac{\phi_{Flare}}{B_R(1\ au)}}$ (top panel); $\sqrt{\phi_{Flare}}$ (middle panel); and A_{Flare} (bottom panel) for 10 flare-produced CMEs. Solid lines represent the line fitting.

contributes greatly to whether the ICME and its preceding shock would encounter Earth, and this is very important as far as the CME's space weather effect is concerned. During the *SOHO* era, what we get from coronagraph's observations is only the projected angular width of the CME that does not represent its real width in 3D space. The GCS model based on the observations of multi-spacecraft of *STEREO* provides a better estimation for the CME's 3D width, which enables us to investigate its relation to the characteristics of the CME's source region.

In this paper, we investigate the correlations between CME's 3D angular width and the characteristics of their source regions (area, flux, etc.) for two kinds of CMEs, i.e., 23 AR-produced CMEs and 10 flare-produced CMEs. We find that for the AR-produced CMEs, their angular widths have some degrees of correlation with the AR's area and magnetic flux. But the correlations are not as high as we expect (with C.C.s between 0.32 and 0.52, *p*-values between 0.1 and 0.01). The magnetic flux within CMEs may come from only part of the ARs, not from the whole. For the flare-produced CMEs, the CME's angular width has stronger correlations with the flare region's area and magnetic flux. Their C.C.s lie between 0.68 and 0.89, and *p*-values between 0.05 and 0.001. The magnetic flux within CMEs seems to be larger than that in the flare regions. Based on these conclusions, we can expect to predict the angular width of the flare-produced CME based on *SDO* data for the flare region as early as the CME just emerges on the Sun. For the AR-produced CMEs, we can at least estimate the upper boundary of the corresponding CME's angular width based on the magnetic observations for the ARs. The relations found in this study can be used to generally predict the CME's 3D angular width directly based on the data for its source region from the space-board and/or ground-based magnetic imagers for the CMEs keeping their constant spatial extents during the propagation in interplanetary space. In other words, we can coarsely predict the width of a CME just based on the magnetic data for its source region (AR/flare) before the CME's eruption. The obtained angular width can be used as a good reference to judge the geoeffectiveness of the specified region (AR or flare) on the Sun in the context of space weather.

This work is jointly supported by the National Natural Science Foundation of China (41231068, 41474153, 41531073, 41374176, 41731067, 41274179, and 41674170), the Youth Innovation Promotion Association CAS under grant No. 2016133, and the Natural Science Foundation of Jiangsu Province (BK20140994). The *STEREO*/SECCHI/COR2 CME catalog is generated and maintained at the Institute for Astrophysics of the University of Goettingen, supported by the German Space Agency DLR and the European Union in collaboration with the U.S. Naval Research Laboratory, Washington. We acknowledge the use of HMI and AIA data of *SDO* and the in situ data of *Wind* spacecraft. We thank Dr. Jie Chen and Dr. Chaowei Jiang for beneficial discussions. We dedicate this paper to the memory of our beloved Professor Shi-Tsan Wu at UAH. We were all saddened by his sudden passing.

ORCID iDs

X. H. Zhao https://orcid.org/0000-0002-9977-2646
X. S. Feng https://orcid.org/0000-0001-8605-2159

References

Bobra, M. G., Sun, X., Hoeksema, J. T., et al. 2014, SoPh, 289, 3549
Bosman, E., Bothmer, V., Nistico, G., et al. 2012, SoPh, 281, 167
Burlaga, L., Sittler, E., Mariani, F., & Schwenn, R. 1981, JGR, 86, 6673
Cane, H. V., Richardson, I. G., St., & Cyr, O. C. 2000, GeoRL, 27, 3591
Chen, C. X., Wang, Y. M., Shen, C. L., et al. 2011a, JGR, 116, A12108
Chen, J., Bao, S. D., & Zhang, H. Q. 2006, SoPh, 235, 281
Chen, J., Lundstedt, H., Deng, Y. Y., Wintoft, P., & Zhang, Y. 2011b, SoPh, 273, 51
Dryer, M. 1994, SSRv, 67, 363
Gopalswamy, N., Yashiro, S., Kaiser, M. L., et al. 2001, JGR, 106, 29219
Gosling, J. T. 1993, JGR, 98, 18937

Green, L., & Baker, D. 2015, Wthr, 70, 31
Kahler, S., & Gopalswamy, N. 2009, Proc. ICRC, 31, 266
Kahler, S. W. 2004, ApJ, 603, 330
Kahler, S. W., Sheeley, N. R., & Liggett, M., J. R. 1989, ApJ, 344, 1026
Kahler, W. W. 2005, ApJ, 628, 1014
Kim, H., Moon, Y.-J., Jang, M., et al. 2008, JKAS, 41, 181
Klimchuk, J., Acton, L., Harvey, K., et al. 1994, in X-ray Solar Physics from Yohkoh, ed. Y. Uchida et al. (Tokyo: Universal Academy), 181
Kwon, R.-Y., Zhang, J., & Vourlidas, A. 2015, ApJ, 799, L29
Moore, R. L., Sterling, A. C., & Suess, S. T. 2007, ApJ, 668, 1221
Pan, Z. H., Wang, C. B., Wang, Y. M., & Xue., X. H. 2011, SoPh, 270, 593
Pick, M. T., Forbes, G., Mann, G., et al. 2006, SSRv, 123, 341
Raymond, J. C., Thompson, B. J., St., Cyr, O. C., et al. 2000, GeoRL, 27, 1439
St. Cyr, O. C., Howard, R. A., Sheeley, N. R., et al. 2000, JGR, 105, 18169
Thernisien, A. F. R., Howard, R. A., & Vourlidas, A. 2006, ApJ, 652, 763
Vršnak, B., Sudar, D., & Ruzdjak, D. 2005, A&A, 435, 1149
Wang, Y. M., Shen, C. L., Wang, S., & Ye, P. Z. 2004, SoPh, 222, 329
Webb, D. F., Cliver, E. W., Crooker, N. U., et al. 2000, JGR, 105, 7491
Zhao, X. H., Feng, X. S., & Wu, C.-C. 2006, JGR, 111, A09103
Zhao, X. H., Feng, X. S., Xiang, C. Q., et al. 2010, ApJ, 714, 1133